ELSEVIER

Atmospheric Research 86 (2007) 76–87

ATMOSPHERIC RESEARCH

www.elsevier.com/locate/atmos

Aerosol lidar ratio characteristics measured by a multi-wavelength Raman lidar system at Anmyeon Island, Korea

Young M. Noh [a], Young J. Kim [a,*], Byoung C. Choi [b], Toshiyuki Murayama [c]

[a] *Advanced Environmental Monitoring Research Center (ADEMRC), Department of Environmental Science and Engineering, Gwangju Institute of Science and Technology (GIST), Gwangju, Republic of Korea*

[b] *Korea Global Atmospheric Watch Observatory (KGAWO)Meteorological Research Institute (METRI), Anmyeon, Republic of Korea*

[c] *Department of Physics, Tokyo University of Marine Science and Technology, 2-1-6 Etchujima, Koto, Tokyo 135-8533, Japan*

Received 25 October 2006; received in revised form 25 March 2007; accepted 26 March 2007

Abstract

Tropospheric aerosols were investigated with a multi-wavelength Raman lidar system during two measurement periods: March 15th–April 16th, 2004 and May 23rd–June 9th, 2005 at the Korea Global Atmospheric Watch Observatory (KGAWO, 36.32°N, 126.19°E), Anmyeon Island, Korea. The extinction coefficient, backscattering coefficient and lidar ratio (S_a) were measured at 355 and 532 nm with the Raman method. Wavelength-dependent lidar ratio data can be used to determine aerosol type. Average values of S_a were 46.8±6.5 and 71.1±8.2 sr at 355 nm and 49.0±12.2 and 78.6±9.6 sr at 532 nm during the two observation periods in 2004 and 2005, respectively. HYSPLIT backward trajectory analysis showed different pathways of air mass between the two observation periods. Air mass had moved to the measurement site from the Chinese continent by a northwesterly wind in 2004, whereas it moved rather slowly in an easterly direction over the Korean Peninsula in 2005. Raman lidar results obtained in this study can provide useful information on aerosol climatology and aerosol transport characteristics in Northeast Asia.

Keywords: Lidar; Lidar ratio; Aerosol; Raman

1. Introduction

Knowledge of the vertical distribution of atmospheric aerosols and their optical properties is important for determining the direct and indirect radiative forcing of aerosols (Haywood and Ramaswamy, 1998). The largest uncertainty in the retrieval of aerosol optical depth (AOD) from Total Ozone Mapping Spectrometer (TOMS) measurements of backscattered UV light is caused by uncertainty regarding the assumed altitude of the aerosols (Torres et al., 1998). A lidar (LIght Detection And Range) that can measure vertical distribution, an extinction coefficient, and a backscattering coefficient is a useful instrument in atmospheric aerosol research. The need to measure the vertical profile of aerosols has led in part to the use of surface, airborne (Menzies and Tratt, 1997) and space-based lidars (Winker, 1999). Many of these lidars only detect the laser light scattered elastically by molecules and aerosols. Unfortunately, retrieval of aerosol backscatter and extinction profiles from single-wavelength lidar measurements is complicated by the fact that the lidar equation contains two unknowns: the backscatter

* Corresponding author. Tel.: +82 62 970 3401; fax: +82 62 970 3404.
E-mail addresses: nym@gist.ac.kr (Y.M. Noh), yjkim@gist.ac.kr (Y.J. Kim), cbc@kma.go.kr (B.C. Choi), murayama@kaiyodai.ac.jp (T. Murayama).

0169-8095/$ - see front matter © 2007 Elsevier B.V. All rights reserved.
doi:10.1016/j.atmosres.2007.03.006

coefficient and extinction coefficient. In order to obtain an analytical solution to the lidar equation, it has been common practice to assume that these parameters are related in the form of the extinction-to-backscatter ratio or lidar ratio, S_a (Klett, 1981; Fernald, 1984). S_a depends on several factors such as aerosol size, shape, refractive index and relative humidity (RH). On the other hand, Raman lidar measures the extinction coefficient and backscattering coefficient of aerosols simultaneously and independently of each other (Ansmann et al., 1992). Furthermore, no critical assumptions on atmospheric input parameters are needed for data analysis. Raman lidar also provides an unambiguous measurement of the extinction-to-backscatter (lidar) ratio. Multi-wavelength Raman lidar measurements allow the useful characterization of aerosol, and lidar ratios simultaneously measured at two wavelengths have been a useful parameter for the identification of aerosol type (Mattis et al., 2003; Wandinger et al., 2002; Müller et al., 2005). At least two wavelengths are required for calculating the Ångström exponent. Additionally, profile extinction coefficients at 355 and 532 nm and backscattering coefficients at 355, 532 and 1064 nm simultaneously measured by multiwavelength Raman lidar can be used as input parameters to retrieve important microphysical parameters, such as mean (effective) particle radius and single-scattering albedo (Müller et al., 1999a,b; Veselovskii et al., 2002). Since the lidar ratio measured simultaneously at two wavelengths is useful for the identification of aerosol type, this study examined lidar ratio variation at two wavelengths to retrieve information on aerosol characteristics in the Northeast Asian region.

The lidar ratio can be computed as a function of the wavelength of the laser light if the size, composition and shape of the aerosols are known (Ackermann, 1998). Ackermann (1998) modeled S_a values for different tropospheric aerosol types using climatological values of aerosol size distribution to obtain values ranging from 22 ~ 25 sr, 20 ~ 25 sr and 60 ~ 65 sr at 532 nm for maritime, dust and continental aerosols, respectively. The high lidar ratio of continental aerosol with soot content resulted from its absorbing characteristics. However, model computations are inadequate for the correct determination of S_a values when different types of aerosols are internally mixed. Rosen and Kjome (1997) reported that S_a is dependent on altitude and ranges from about 35 to 70 sr from simultaneous observations of nephelometersonde and backscattersonde from the surface up to a 25-km altitude. Franke et al. (2001) found that the lidar ratio was a useful quantity to trace different pollution sources in South and Southeast Asia and reported high lidar ratios at 532 nm of up to 110 sr in the lofted pollution plumes above a 1000-m altitude. Other studies have shown that S_a variation is dependent on regional characteristics of aerosols and atmospheric conditions (Müller et al., 2003; Murayama et al., 2004). Although elastic lidar observations have been conducted at several sites in Korea, including the Korea Global Atmospheric Watch Observatory (KGAWO, Anmyeon island), Jeju Island, Suwon and Gwangju, few direct measurements of S_a have been performed. Direct measurement of S_a using a Raman lidar is needed for a better understanding of the optical characteristics and vertical distribution of atmospheric aerosols over the Korean peninsula, which is located downwind of continental emission sources.

In this study, lidar ratios at two wavelengths were measured with the GIST/ADEMRC (Advanced Environmental Monitoring Research Center of Gwangju Institute of Science and Technology) multi-wavelength Raman lidar system (Hong et al., 2004) during two observation periods, March 15th to April 16th, 2004 and May 24th to June 9th, 2005 at the Korea Global Atmospheric Watch Observatory (KGAWO), Anmyeon Island, which is located 100 km southwest of Seoul and off the mid-west coast of Korea.

2. Observation

The GIST/ADEMRC multi-wavelength Raman lidar system is shown in Fig. 1 and its specifications are summarized in Table 1. The light source is an Nd:YAG laser that emits pulses at 355-nm, 532-nm and 1064-nm wavelengths with a power of 60, 80 and 80 mJ, respectively. The pulse repetition rate is 20 Hz. A λ/2 plate is used to control the light angle incident on the polarizer beam splitter of the receiver unit. The laser beam is expanded 5 times using a beam expander so that the laser beam divergence is controlled to less than 0.2 mrad. The receiver unit of the lidar consists of one 14-inch and two 8-inch Cassegrain telescopes, and seven photomultiplier tubes (PMT) acting as detectors. The seven detectors are used to measure elastic backscattered signals at 355 nm, 532 nm and 1064 nm, horizontal (532S) and perpendicular (532P) polarization signals at 532 nm, and two inelastic atmospheric N_2 Raman backscattered signals at 387 nm and 607 nm. The polarization channels were operated for 24 h and the data were stored in a computer using an analog-to-digital converter (ADC) unit. Polarization signals at 532 nm from backscattering by molecules and aerosols were measured continuously using a 2-channel ADC system

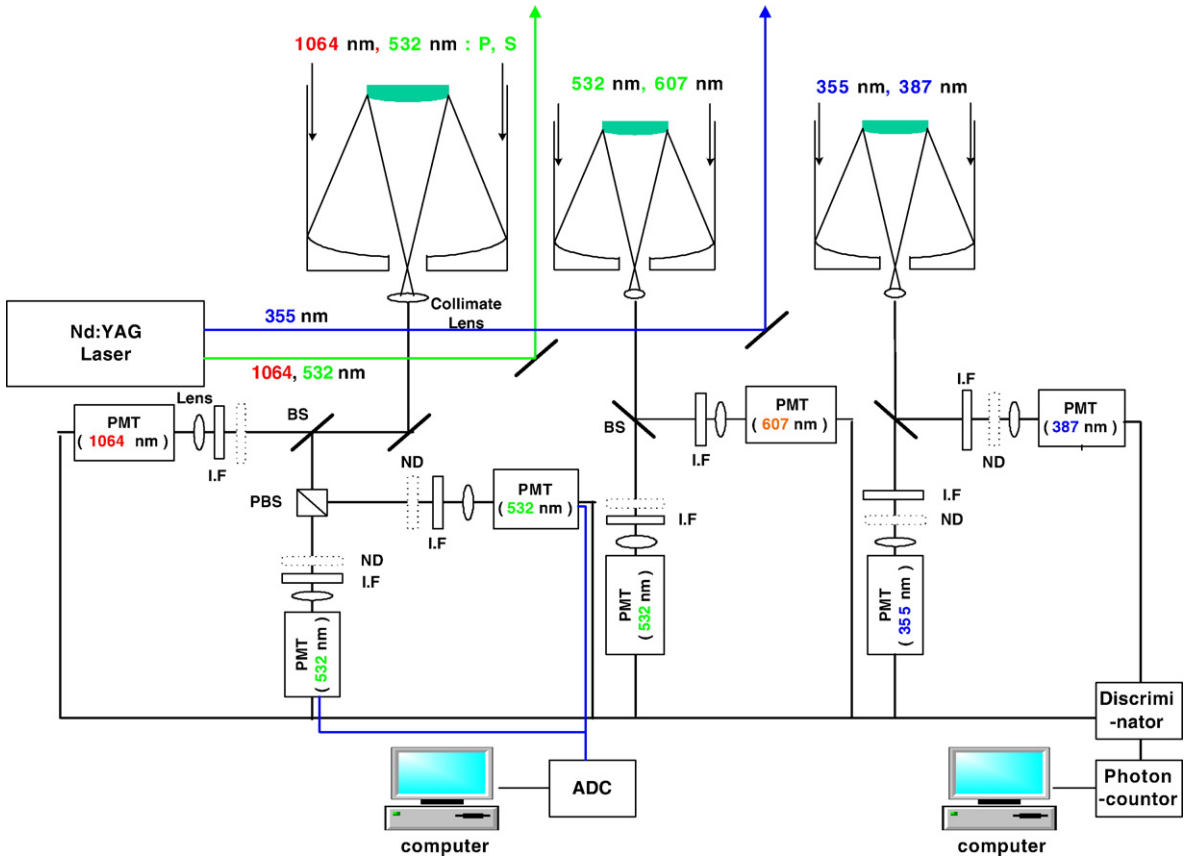

Fig. 1. Schematic diagram of the GIST/ADEMRC multi-wavelength Raman lidar system.

to investigate the vertical distribution and depolarization ratio of atmospheric aerosols. The other five channels used a photon counter system and were operating only during the night time, with data being stored in a computer. Temporal and spatial resolutions were 10 min and 7.5 m, respectively, for both ADC and photon counter systems. 532P and 532S signals of the ADC system were used to determine the depolarization ratio, which is considered an indicator of the aerosol's nonsphericity (Sassen, 1974). Divergent temporal and spatial resolutions were used in data acquisition of Raman signals since they are 10^3–10^4 times weaker than the elastic signals. The spatial resolution was reduced to 120 m for the Raman analysis by summing sixteen data points along the beam path. For the temporal resolution, summation of measured lidar data representing at least 216,000 laser shots (3 h) was necessary to perform Raman data analysis. The Raman lidar signal was normally summed over a period ranging from 3 to 8 h. Only cases involving consistent aerosol layers checked by a time plot of the extinction coefficient calculated by the Klett method over a 20-minute temporal resolution were included in the summation. Raman analysis was not performed if the consistent aerosol layer was detected for less than 3 h or showed wide variation in height and optical depth. In the case of aerosol optical depth, variation of less than +/−0.05 was included for the above process. The systematic error due to variations of optical depth during the data summation period was less than 5% by above process when optical depth was 0.3 at 532 nm.

The aerosol backscatter coefficient, extinction coefficient, and lidar ratio at 355 and 532 nm were determined from the elastic and inelastic return signals according to the method described by Ansmann et al. (1990, 1992) and Whiteman et al. (1992). Radiosonde data collected about 5 km from the lidar site provided information on the vertical profiles of pressure, temperature and relative humidity, which allowed an accurate correction of the Rayleigh scattering effects on the signals. Based on the 'Error propagation equation' (Bevington and Robinson, 1992), typical statistical errors for the determination of the aerosol backscattering coefficient, extinction coefficient and lidar ratio in the middle part of the observed aerosol layers were 5–15%, 5–15% and 15–30%, respectively. The main error

Table 1
GIST/ADEMRC multi-wavelength Raman lidar system

Laser	
Type	Nd:YAG Laser (CFR 400 Big Sky Laser)
Wavelength	355, 532, 1064 nm
Pulse energy	60 mJ (at 355 nm), 80 mJ (at 532 and 1064 nm)
Repetition rate	20 Hz
Beam Divergence	0.2 mrad after 5X beam expanding
Pulse duration	<10 ns
Receiver optics	
Optical design	Two 8-inch and one 14-inch Schmidt–Cassegrain telescope
Focal length	3910 mm (14 in. telescope), 2032 mm (8-inch telescope)
Field of view	0.5–4.0 mrad (changeable)
Dispersion system	
Wavelength (nm)	[1064, 532P, 532S (14 in.)]/[532, 607 (1st 8 in.)]/[355, 387 (2nd 8 in.)]
Interference filter bandwidth (nm)	[1.06, 0.18, 0.21 (14 in.)]/[0.97, 1.3 (1st 8 in.)]/[9.19, 0.72 (2nd 8 in.)]
Interference filter peak transmittance (%)	[42.65, 47.57, 46.95 (14 in.)]/[53.68, 38.2 (1st 8 in.]/[29.15, 13.76 (2nd 8 in.)]
Detector	PMT (HAMAMATSU R3234-01 for 355, 387, 532, 607 and R3236 for 1064)
Data acquisition system	
Photon counting system	8 channel Photon counting system
Maximum count rate	300 MHz,
Maximum sampling rate	20 MHz (7.5 m)
ADC system	PCI type
A/D resolution	12 bit
Maximum sampling rate	65 MHz

source is the signal noise. The aerosol layers were classified using aerosol extinction coefficients and meteorological conditions such as ambient temperature and RH obtained by radiosonde. The aerosol optical depth (AOD, τ) at 355 nm and 532 nm of each classified aerosol layer was calculated by integrating the aerosol extinction coefficient. The Ångström exponent ($\ddot{a}$) was calculated using acquired AOD values at 355-nm and 532-nm wavelengths.

$$\ddot{a} = -\frac{\ln(\tau_{355}/\tau_{532})}{\ln(355/532)}$$

3. Results

Range-corrected, backscatter signals acquired from continuous measurements using an ADC system from March 15th to April 16th, 2004 and May 24th to June 9th, 2005 are shown in Figs. 2 and 3, respectively. The black color in these figures represents the strong backscatter signal resulting from the presence of clouds, while the green color represents atmospheric aerosols. The blue and white colors represent clean atmospheric conditions. No observations were made during rainy days. Fig. 2 shows variations in the vertical distribution of aerosol during the 2004 observation period. Most aerosols were detected below a 3-km altitude during the 2005 measurement period, as seen in Fig. 3. The number of days on which the lidar ratio was estimated at both 355-nm and 532-nm wavelengths was 6 and 11 in 2004 and 2005, respectively. Since the full overlap height was as high as 1–2 km during the 2004 period, an aerosol extinction profile was obtained only above that height using the 387-nm Raman scattered signal. The overlap height of the lidar system was improved to 0.6 km by reducing the size of the telescope iris and the distance between the telescope and laser source during the 2005 measurement period. The overlap profile was checked by the direct method (Wandinger and Ansmann, 2002) using the data observed on the cleanest day, which was June 1st, 2005. The overlap factor was 1 above 0.6 km at 532 nm. However, full overlap did not occur up to 3 km at 355 nm. For this reason, an overlap correction was performed for the extinction coefficient calculation at 355 nm.

The height of the aerosol layer can be determined from the vertical profiles of aerosol backscattering coefficient, potential temperature and RH obtained by radiosonde. Knowledge of the potential temperature lapse rate is usually sufficient for determining static stability (Stull, 1988). The region where the aerosol backscattering coefficient sharply decreases and the potential temperature lapse rate varies has been determined as the top of the PBL. The small differences of layer height between lidar and radiosonde results can be ascribed to differences in measurement sites and measurement periods (Cooper and Eichinger, 1994; Santacesaria et al., 1998). The top of the PBL altitude was within a 1.2–3.0-km range during the lidar measurement periods of the current study. Profiles of the lidar ratio and Ångström exponent can also be determined from aerosol extinction and backscattering profiles. When multiple aerosol layers existed above the measurement site, the average lidar ratio and Ångström exponent of each layer were calculated separately. Examples of vertical profiles of aerosol backscattering coefficient and lidar ratio are shown in Figs. 4 and 5. Fig. 4(a) shows vertical distributions of calculated aerosol backscattering coefficients at 355 nm and 532 nm, as

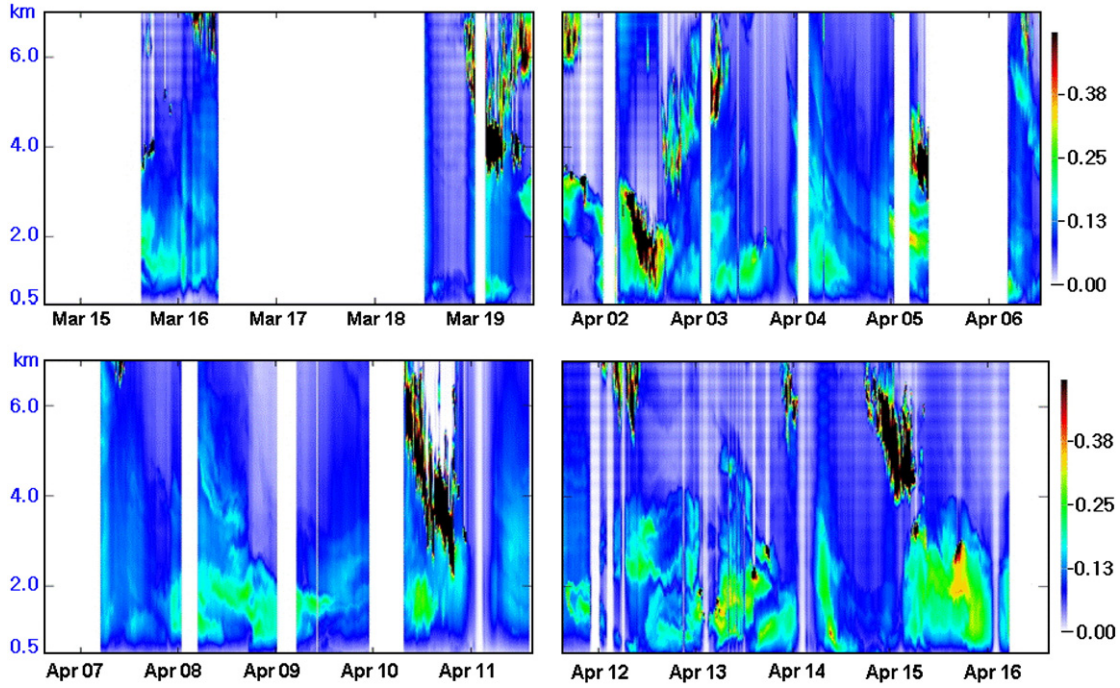

Fig. 2. Range-corrected signal of 532 nm recorded with the ADC system from March 15th to April 16th, 2004 at Anmyeon Island.

well as those of potential temperature and RH obtained from radiosonde data. The potential temperature profile shows that the top of the PBL was ~3.0 km, as evidenced by lapse rate change at that region. The height of PBL determined from the temperature profile obtained by radiosonde was in good agreement in the most cases with that determined from the aerosol profile based on lidar measurements as shown in Figs. 4 (a) and 5 (a). The small

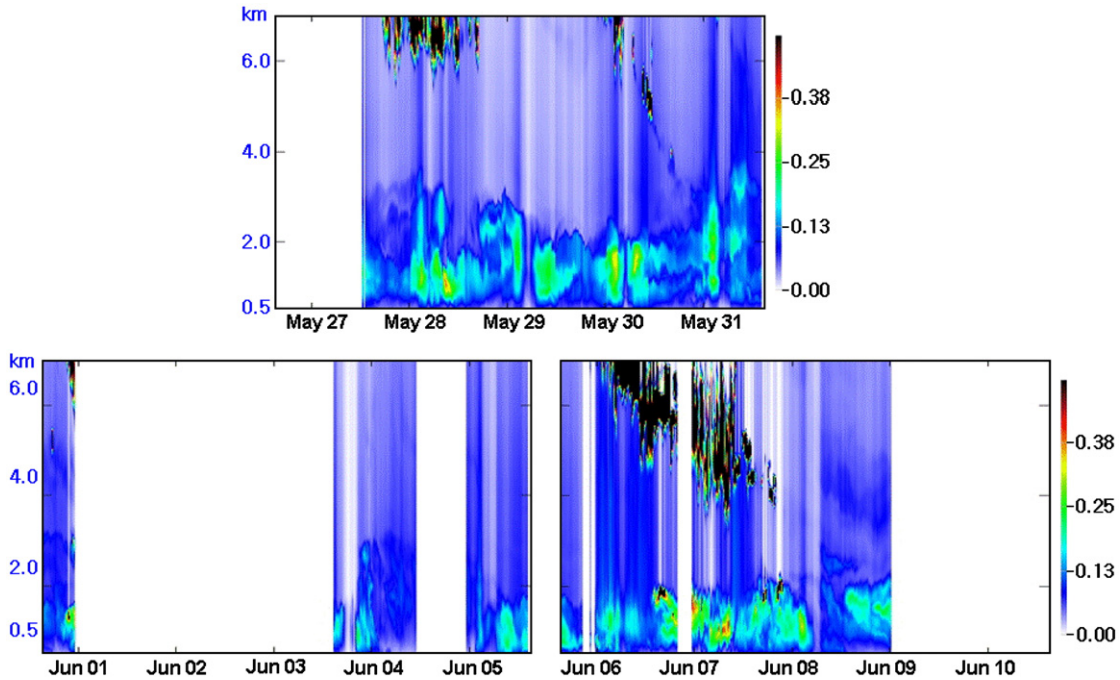

Fig. 3. Range-corrected signal of 532 nm recorded with the ADC system from May 24th to June 8th, 2005 at Anmyeon Island.

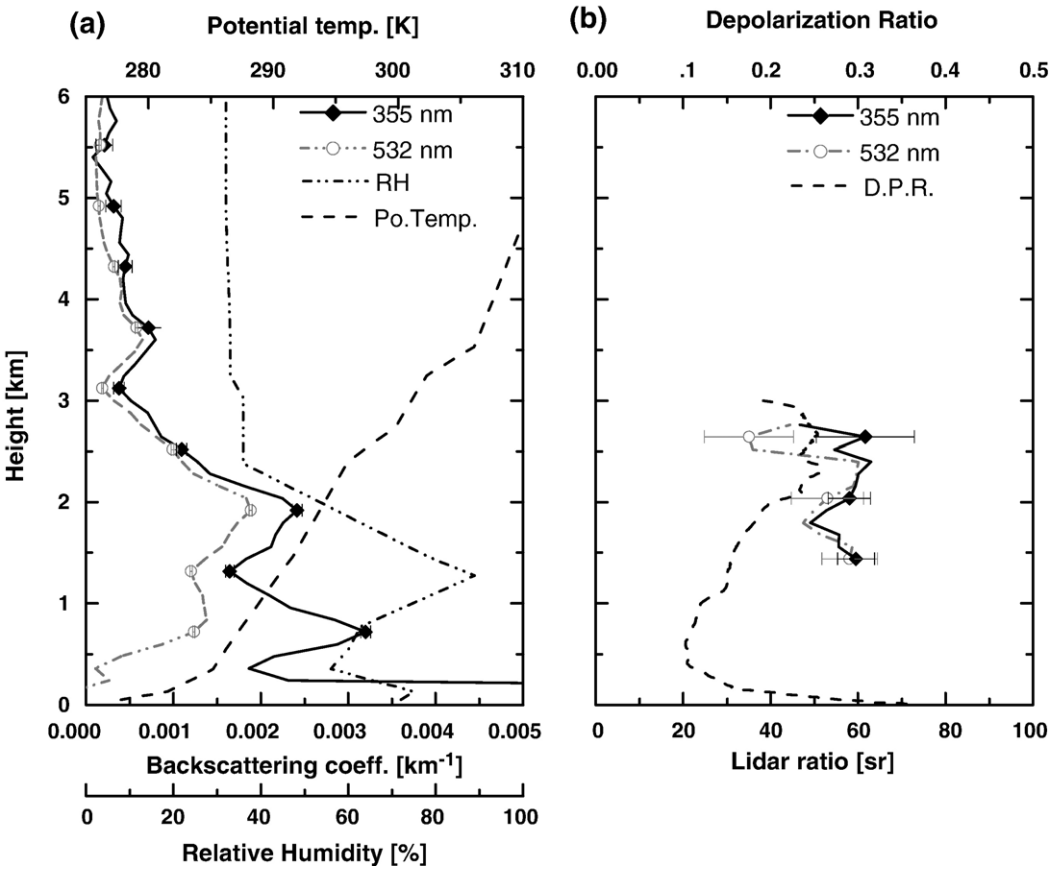

Fig. 4. Raman analysis and radiosonde results obtained from April 8th 22:01 to 9th 05:24, 2004. (a) Backscattering coefficient based on Raman lidar measurements at 355 and 532 nm, with potential temperature and relative humidity values gathered by radiosonde. (b) Lidar ratio at 355 and 532 nm, including depolarization ratio derived from Raman lidar data.

differences between the two methods can be ascribed to the different locations of the measurements. Retrieval of the aerosol extinction profile was only performed above 1 km, where the laser beam is fully within the telescopic field-of-view. In Fig. 4(a), the aerosol layer was present within the altitude range of 1.2–3.0 km. Relative humidity was 60–90% in the PBL, but decreased to a low of 40% above the PBL. The lidar ratio and depolarization ratio of the aerosol layer as shown in Fig. 4(b) were around 60 sr at both wavelengths and 0.15–0.25, respectively, which are quite reasonable. The observed aerosol layer was identified as Asian dust by its high depolarization ratio of 0.15–0.25 (Murayama et al., 2004; Sakai et al., 2003). The average Ångström exponent (355–532 nm) value of the aerosol layer was 0.65, which suggests that the aerosol is mostly composed of coarse-mode particles. Fig. 5(a) and (b) present data obtained from 20:08, 30 May to 05:42, 31 May 2004 in the same manner as data shown in Fig. 4 and reveal that the observed optical characteristics of aerosol differ from those shown in Fig. 4. The depolarization ratio reached a low value of 0.09 and the Ångström exponent is as high as 1.59. Additionally, the lidar ratio exhibits a spectral behavior that differs from that shown in Fig. 4. These results suggest that the aerosol mostly consisted of fine light-absorbing particles.

Average lidar ratios at 355 and 352 nm computed for each aerosol layer observed during the entire study period are shown in Fig. 6. The average lidar ratio was computed between the minimum and maximum altitudes of the aerosol layer. Optical depth (τ), height of the observed aerosol layer, the Ångström exponent, and depolarization ratio of each aerosol layer are summarized in Table 2.

The backward trajectory was conducted to find the source region of the aerosols. The NOAA/ARL Hybrid Single-Particle Lagrangian Integrated Trajectory (HYSPLIT; Draxler and Rolph, 2003) model (http://www.arl.noaa.gov/ready/open/hysplit4.html) was used to calculate the five-day backward trajectories of air masses.

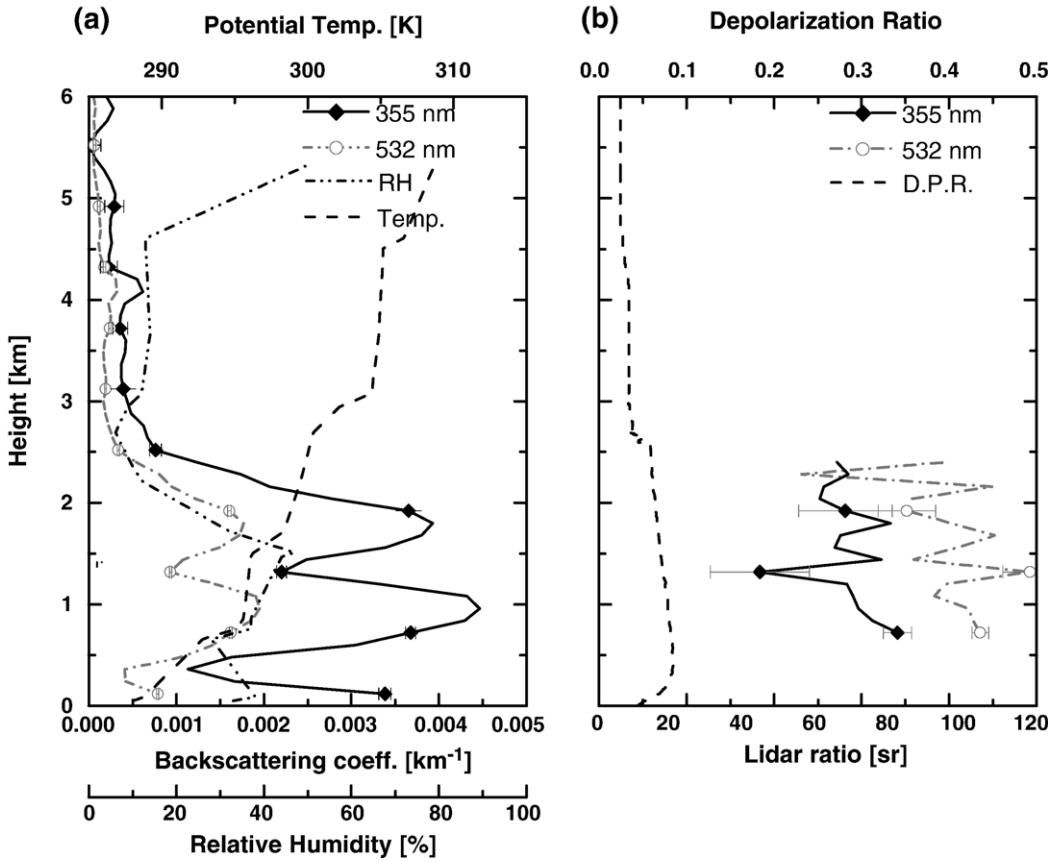

Fig. 5. Raman analysis and radiosonde results recorded from May 30th 20:08 to 31st 05:42, 2005. (a) Backscattering coefficient based on Raman lidar measurements at 355 and 532 nm, with potential temperature and relative humidity values gathered by radiosonde. (b) Lidar ratio at 355 and 532 nm, including and depolarization ratio derived from Raman lidar data.

Three arrival points were selected between a 1000 and 4000-m height according to the location of aerosol layers in 2004. The height of the start point for 2005 data was fixed at 1000, 1500 and 2000 m since most of the aerosol layers were detected below 2000 m. Pathways of air masses that arrived above Anmyeon Island during the observation periods were categorized into four types, as shown in Fig. 7. Averaged optical properties of aerosol for the different air mass pathway types are summarized in Table 3. Air mass pathway type (a) includes the entire observation period in 2004, with the exception of April 3. Air masses came from western and northwestern China and most of the aerosol layers were detected above the PBL. Aerosol observed during the type (a) period was mostly dust aerosol, which resulted in a high depolarization ratio between 0.21 and 0.38 and a low Ångström exponent of 0.58–1.00. Average values of the depolarization ratio and Ångström exponent were 0.26±0.10 and 0.78±0.20, respectively. Average values of the lidar ratio were 47.1±7.0 and 45.5±8.6 sr at 355 and 532 nm, respectively. Optical properties of Asian dust observed above the PBL in Korea showed little variation due to the lack of opportunity for mixing during transport between dust and anthropogenic pollutants mostly present in the PBL.

Air mass moved from northeastern China during the type (b) period, as shown in Fig. 7(b). The type (c) air mass pattern as shown in Fig. 7(c) represents a slow movement and stagnant pattern of air mass over the West Sea. These two types were detected only for a few cases; 2 days for type (b) and 1 day for type (c).

Type (d) air masses slowly moved from the East Sea and stagnated over the Korean Peninsula. Unlike the type (a) case, most aerosols existed in the PBL during the type (d) periods. No case of Asian dust was observed during this observation period. A higher lidar ratio was observed at both wavelengths, with average values of 73.2±7.5 sr and 81.5±7.6 sr at 355 and 532 nm, respectively. The lidar ratio at 532 nm was higher by an

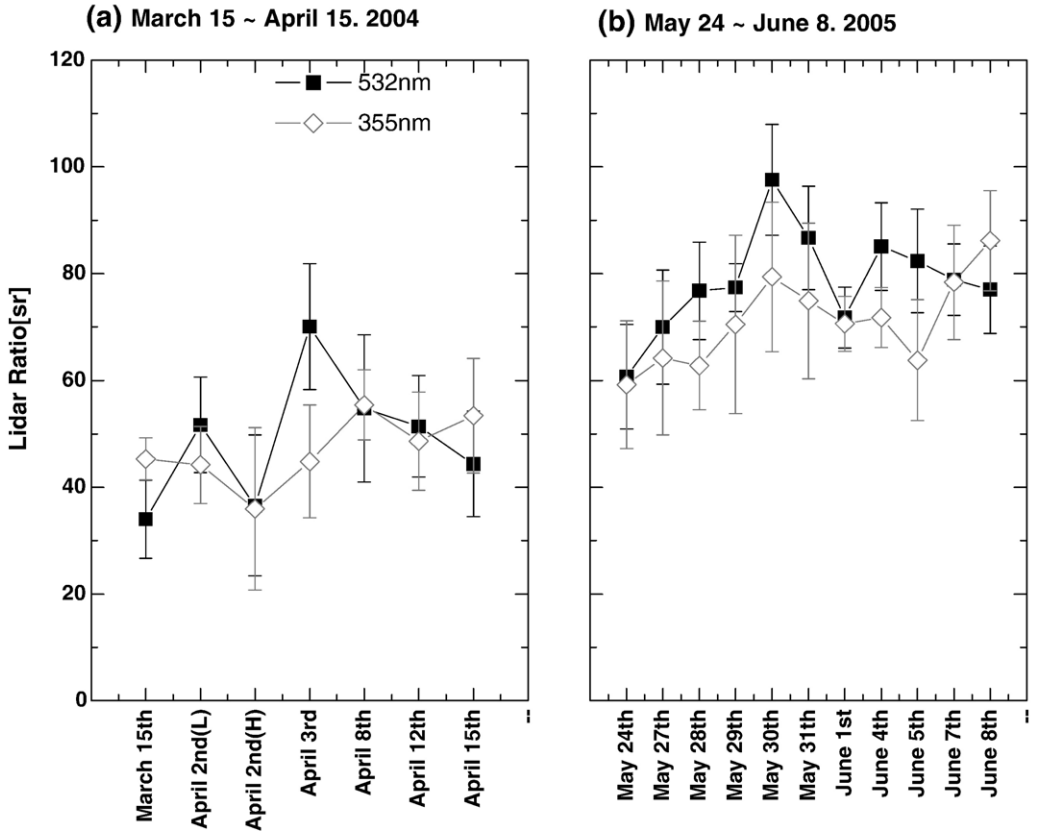

Fig. 6. Average lidar ratios of aerosol layers at 355 and 532 nm. (a) Thirteen cases observed from 24th May to 8th June, 2005. (b) Eight cases observed from 15th March to 8th April, 2004.

average of 8.3 sr than that at 355 nm. These differences in lidar ratio between type (a) and (d) air masses might have resulted from differences in aerosol type, origin and transporting altitude. Backward trajectory results of type (d) periods showed that the unusually high lidar ratio was related to a slowly moving or stagnant air mass pattern around the Korean peninsula. The aerosols observed during type (d) were believed to be a mixture of anthropogenic aerosol and smoke aerosols from forest fires and/or biomass burning. In Korea, open field burning of agricultural waste after the harvest of barley is commonly practiced in late spring (Ryu et al., 2004).

In-situ measurements of black carbon (BC) and SO_2 using an aethalometer and fluorescence SO_2 analyzer were made simultaneously at the Korea Global Atmospheric Watch Observatory (KGAWO) site. The BC-to-SO_2 ratio is indicative of the light absorption-to-scattering ratio of particles (Franke et al., 2001). This ratio is compared with variation of the lidar ratio. The average value of the BC-to-SO_2 ratio was higher in 2005 (1.26) than 2004 (0.62). It is known that a higher absorption-to-scattering ratio of aerosol is associated with a higher lidar ratio for aerosol with similar size-distribution characteristics (Müller et al., 2001a,b). Aerosols observed in 2005 were smaller in size than those recorded in 2004, as evidenced by the higher average values of the Ångström exponent: 1.46±0.30 (2005) vs. 0.79±0.18 (2004). Comparisons of lidar ratios observed in this study with those of previous studies are summarized in Table 4. Sakai et al. (2002) reported comparable lidar ratio values for Asian dust aerosol over Tsukuba, Japan. Based on the observed lidar ratios at two wavelengths, the aerosol type can be separated according to the variation of the lidar ratio (Murayama et al., 2004). Our lidar ratios recorded in 2005 were compared with those of a biomass burning plume observed at Leipzig (51.3°N, 12.4°E), Germany (Müller et al., 2005). Mean lidar ratios representing biomass burning plumes were lower at 355 nm than at 532 nm. Similar spectral behavior was reported for dual-wavelength Raman lidar observations of Siberian biomass-burning aerosol detected over Tokyo, Japan (Murayama et al., 2004) and for biomass-burning aerosol advected from Canada to Germany (Wandinger

Table 2
Optical characteristics of each aerosol layer observed with the Multi-wavelength Raman lidar system

Year	Date	Height (km)	τ		$\ddot{a}$ [a]	DPR [a]	Lidar ratio (sr)	
			532 nm	355 nm			532 nm	355 nm
2004	March 15th	2.10–3.42	0.08	0.12	1.00	0.30±0.05	34.0±7.3	45.3±3.9
	April 2nd (L) [b]	1.02–2.34	0.27	0.38	0.87	0.10±0.01	51.7±9.0	44.2±7.2
	April 2nd (H) [b]	3.06–5.70	0.31	0.39	0.58	0.31±0.07	36.6±13.2	35.9±15.2
	April 3rd	1.14–2.22	0.14	0.19	0.84	0.08±0.01	70.1±11.8	44.8±10.6
	April 8th	1.44–3.00	0.11	0.14	0.65	0.21±0.04	54.8±13.8	55.4±6.6
	April 12th	2.34–4.26	0.17	0.21	0.60	0.38±0.07	51.4±9.5	48.6±9.2
	April 15th	1.86–3.54	0.22	0.33	1.00	0.26±0.06	44.4±9.9	53.4±10.7
	Average		0.18	0.25	0.79	0.23±0.11	49.0±12.2	46.8±6.5
2005	May 24th	1.72–3.18	0.15	0.24	1.18	0.07±0.02	60.7±9.8	59.2±12.0
	May 27th	0.66–3.18	0.34	0.69	1.78	0.08±0.01	70.0±10.7	64.2±14.4
	May 28th	0.66–2.82	0.34	0.56	1.25	0.07±0.03	76.8±9.1	62.8±8.3
	May 29th	0.66–2.34	0.44	0.81	1.51	0.10±0.02	77.4±4.5	70.5±16.7
	May 30th	0.66–2.22	0.23	0.43	1.59	0.06±0.01	97.6±10.4	79.4±14.0
	May 31st	0.66–1.50	0.09	0.21	2.08	0.06±0.01	86.7±9.7	74.9±14.6
	June 1st	1.26–1.86	0.05	0.10	1.48	0.08±0.01	71.8±5.7	70.6±5.1
	June 4th	0.66–1.86	0.16	0.11	1.01	0.10±0.02	85.1±8.2	71.8±5.6
	June 5th	0.66–2.10	0.21	0.35	1.21	0.09±0.02	82.4±9.7	63.8±11.3
	June 7th	0.78–1.62	0.20	0.34	1.36	0.08±0.01	78.9±6.7	78.4±10.7
	June 8th	0.66–1.86	0.16	0.31	1.56	0.06±0.01	77.0±8.2	86.2±9.4
	Average		0.22	0.38	1.46	0.08±0.01	78.6±9.6	71.1±8.2

[a] $\ddot{a}$ and DPR denote the Ångström exponent based on optical data at 355 and 532 nm and depolarization ratio, respectively.
[b] L and H denote different aerosol layers observed at the same time.

et al., 2002). However, our results are much higher than those presented in the aforementioned studies. A high lidar ratio of up to 110 sr at 532 nm was detected above a 1000-m height for the heavily polluted air transported from India and Southeast Asia (Franke et al., 2001). Moreover, the lidar ratio increased as the ratio of fine to coarse-mode particles increased (Ferrare et al., 2001). The unusually high lidar ratios observed in 2005 were considered a result of the increased influence of the absorption of relatively small-size particles of anthropogenic aerosol mixed with a biomass burning plume under stagnant atmospheric conditions.

4. Conclusion

Aerosol optical properties were measured using a multi-wavelength Raman lidar system developed by GIST/ADEMRC, Korea during two study periods, March 15th–April 16th, 2004 and May 23rd–June 9th, 2005 at Anmyeon Island, KGAWO (36.32°N, 126.19°E), Korea. Vertical profiles of the extinction coefficient, backscattering coefficient, and the lidar ratio were obtained at 355 and 532 nm using the Raman method. The characteristics of aerosol layers were determined using optical properties, such as the lidar ratio and Ångström exponent. The average lidar ratio differed between the two observation periods: 46.8±6.5 sr and 49.0±12.2 sr at 355 nm and 532 nm, respectively, in 2004 versus 71.1±8.2 sr and 78.6±9.6 sr at 355 nm and 532 nm, respectively, in 2005. The difference in lidar ratio between the two periods corroborated the difference in average Ångström exponent of 0.79±0.18 in 2004 and 1.46±0.30 in 2005.

The observed differences in lidar ratio and Ångström exponent between the two observation periods are the result of differences in the origin of the aerosols. Combined analyses of Raman lidar observations, in-situ measurements, backward trajectories and sunphotometer observations suggested that the aerosols observed in 2004 were mostly long-range transported dust aerosols from the Asian continent. A lidar ratio of less than 60 sr at 532 nm was observed for most cases, which is consistent with the results of Asian dust cases observed in Japan (Murayama et al., 2004). This suggests that Asian dust particles originated from a source region and that movement above the PBL produced little change in their optical properties during their transport in Northeast Asia. In contrast, most of the aerosols observed in 2005 exhibited unusually high lidar ratios of up to 79.4 and 97.6 sr at 355 and 532 nm, respectively, which resulted from the influence of light-absorbing aerosols consisting of a mixture of anthropogenic and biomass burning aerosol that moved from an easterly direction under stagnant atmospheric conditions. The high absorption characteristics of aerosols observed in 2005 can also be confirmed by the observed BC-to-SO_2 ratio. The results of backward trajectory

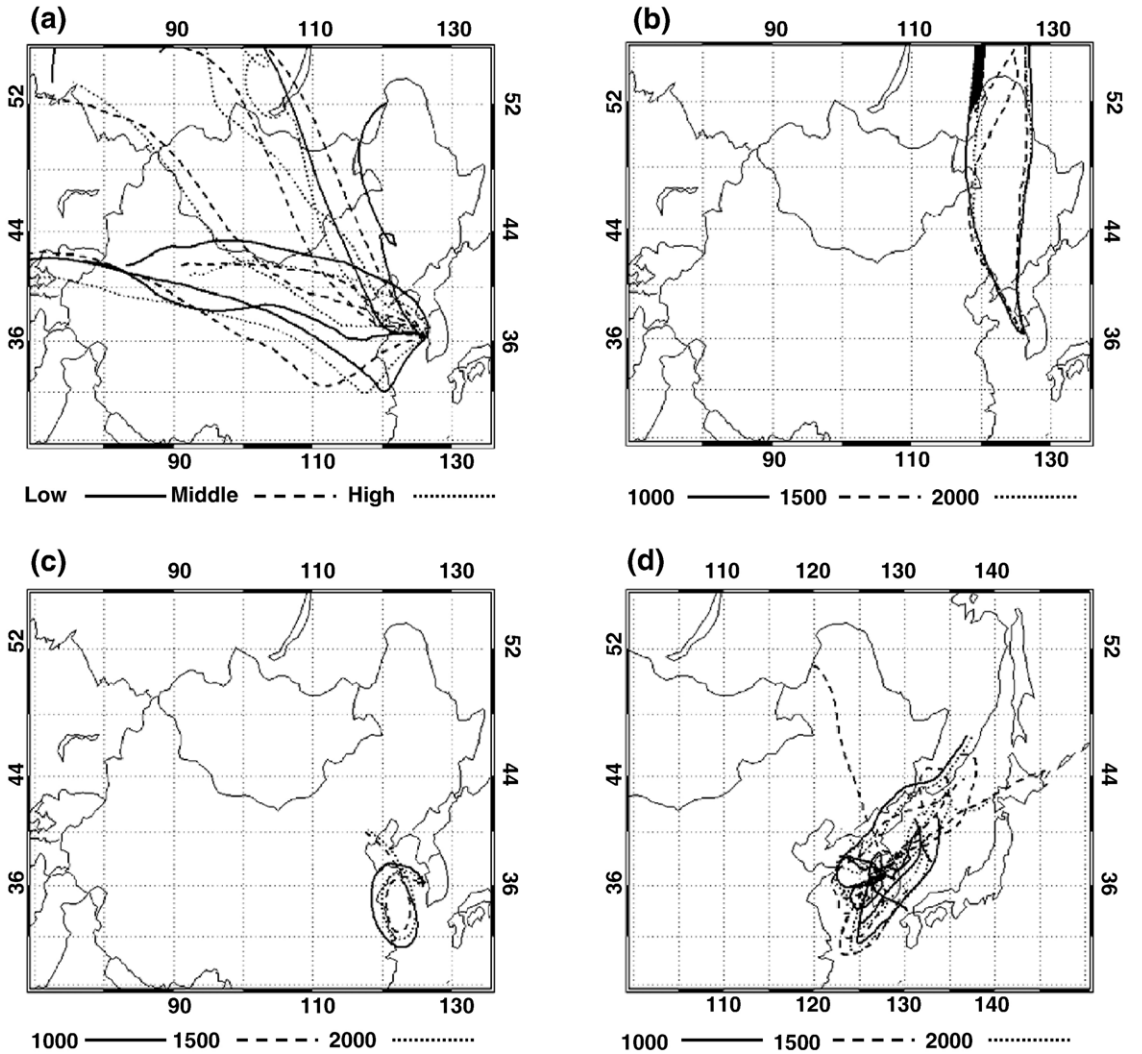

Fig. 7. Five-day backward trajectory by NOAA/ARL HYSPLIT-4. (a) Air masses moved from western and northwestern china. Low: 1000–2500 m, Middle: 2500–3000 m, High: 3000–4000 m (b) Air masses moved from northeastern china across Korea. (c) Air masses stagnant around the West Sea. (d) Air masses moved from east and stagnant around the Korean Peninsula.

analysis of aerosol air masses indicated that they had been directly advected from an Asian dust source region in 2004, whereas they were rather stagnant around the Korean peninsular in 2005.

We conclude that the wavelength dependence of the lidar ratio can be utilized to distinguish aerosol types in remote sensing. Large differences between long-range transported aerosols originated from China and inner

Table 3
Average optical values for different backward trajectory patterns

Pattern	Date	ä	DPR	Lidar ratio (sr)	
				532 nm	355 nm
a	March 15th, April 2nd (L and H), 8th, 12th, 15th, 2004	0.78±0.20	0.26±0.10	45.5±8.6	47.1±7.0
b	April 3rd 2004, May 24th, 2005	1.01±0.24	0.08±0.01	65.4±6.6	52±10.2
c	May 27th 2005	1.78	0.08	70.0	64.2
d	May 28th, 29th, 30th, 31st, June 1st, 4th, 5th, 7th, 8th, 2005	1.45±0.30	0.08±0.02	81.5±7.6	73.2±7.5

Table 4
Lidar ratios at 532 nm and 355 nm for different types of aerosol

Aerosol type	Lidar ratio (sr)	Wavelength (nm)	Region	Reference
Asian Dust	47±18	532	Tokyo, Japan	Sakai et al. (2003)
	48.6±8.5	355		Murayama et al., (2004)
	43.1±7.0	532		
	42–55	532		Liu et al. (2002)
	47.1±7.0	355	Anmyeon Island, Korea	This study (2004)
	45.5±8.6	532		
Continental aerosol	68±12	355	Oklahoma, U.S.A.	Ferrare et al. (200)
Haze	46.7±5.6	532	Southeast, China	Ansmann et al. (2005)
Forest fire smoke	37.9±13.1	355	Leipzig, Germany	Müller et al. (2005)
	52.3±16.6	532		
Arctic haze mixed with urban aerosol	35–75	355	Leipzig, Germany	Müller et al. (2004)
		532		
Smoke plume	~40	355	Tokyo, Japan	Murayama et al. (2004)
	~60	532		
Pollution plume	~110	532	Indian Ocean	Franke et al. (2001)
Anthropogenic	71.1±8.2	355	Anmyeon Island, Korea	This study (2005)
	78.6±9.6	532		

Mongolia, and accumulated pollution aerosols mixed with biomass burning aerosol under stagnant atmospheric conditions were detected in this study. Variation of the lidar ratio in relation to aerosol type can be used to detect particle light-absorbing characteristics. Thus, the results of this investigation revealed that Raman lidar measurements can provide useful information on aerosol climatology and aerosol transport characteristics in Northeast Asia. A future study might involve the investigation of microphysical properties, including the refractive index and single-scattering albedo, as well as a study of aerosol optical properties using the GIST multi-wavelength Raman lidar system in order to obtain more detailed information about aerosol characteristics in Northeast Asia.

Acknowledgements

This work was supported by the Korea Meteorological Administration Research and Development Program under Grant CATER 2007-4108. This research was partially supported by the Brain Korea 21(BK21) program for the fellowship Young M. Noh.

References

Ackermann, J., 1998. The extinction-to-backscattering ratio of tropospheric aerosol: a numerical study. J. Atmos. Ocean. Technol. 15, 1043–1050.

Ansmann, A., Wandinger, U., Riebesell, M., Weitkamp, C., Michaelis, W., 1990. Measurement of atmospheric aerosol extinction profiles with a Raman lidar. Opt. Lett. 15, 746–748.

Ansmann, A., Wandinger, U., Riebesell, M., Weitkamp, C., Michaelis, W., 1992. Independent measurement of extinction and backscatter profiles in cirrus clouds by using a combined Raman elastic-backscatter lidar. Appl. Opt. 31, 7113–7131.

Ansmann, A., Engelmann, R., Althausen, D., Wandinger, U., 2005. High aerosol load over Pearl River Delta, China, observed with Raman lidar and Sun photometer. Geophys. Res. Lett. 32, L13815.

Bevington, R.P., Robinson, D.K., 1992. Data Reduction and Error Analysis for the Physical Sciences. McGraw-Hill, Inc., pp. 38–51.

Cooper, D.I., Eichinger, W.E., 1994. Structure of the atmosphere in an urban planetary boundary layer from lidar and radiosonde observations. J. Geophys. Res. 99, 22937–22948.

Draxler, R.R., Rolph, G.D., 2003. HYSPLIT (Hybrid Single-Particle Lagrangian Integrated Trajectory) Model Access via NOAA ARL READY Website. NOAA Air Resources Laboratory, Silver Spring, MD. http://www.arl.noaa.gov/ready/hysplit4.html.

Fernald, F.G., 1984. Analysis of atmospheric lidar observations: some comments. Appl. Opt. 23, 652–653.

Ferrare, R.A., Turner, D.D., Brasseur, L.H., Feltz, W.F., Dubovik, O., Tooman, T.P., 2001. Raman lidar measurements of the aerosol extinction-to-backscatter ratio over the Southern Great Plains. J. Geophys. Res. 106, 20333–20347.

Franke, K., Ansmann, A., Müller, D., Althausen, D., Wagner, F., Scheele, R., 2001. One-year observations of particle lidar ratio over the tropical Indian Ocean with Raman lidar. Geophys. Res. Lett. 28, 4559–4562.

Haywood, J.M., Ramaswamy, V., 1998. Global sensitivity studies of the direct radiative forcing due to anthropogenic sulfate and black carbon aerosols. J. Geophys. Res. 103, 6043–6058.

Hong, C.S., Lee, K.H., Kim, Y.J., Iwasaka, Y., 2004. Lidar measurements of the vertical aerosol profile and optical depth during the ACE-Asia 2001 IOP, at Gosan, Jeju Island, Korea. Environ. Monit. Assess. 92, 43–57.

Klett, J.D., 1981. Stable analytical inversion solution for processing lidar returns. Appl. Opt. 20 (2), 211–220.

Liu, Z., Sugimoto, N., Murayama, T., 2002. Extinction-to-backscatter ratio of Asian dust observed with high-spectral-resolution lidar and Raman lidar. Appl. Opt. 41, 2760–2767.

Mattis, I., Ansmann, A., Wandinger, U., Müller, D., 2003. Unexpectedly high aerosol load in the free troposphere over

central Europe in spring/summer 2003. Geophys. Res. Lett. 30, 2178, doi:10.1029/2003GL018442.

Menzies, R.T., Tratt, D.M., 1997. Airborne lidar observations of tropospheric aerosols during the Global Backscatter Experiment (GLOBE) Pacific circumnavigation missions of 1989 and 1990. J. Geophys. Res. 102 (3), 3701.

Müller, D., Wandinger, U., Ansmann, A., 1999a. Microphysical particle parameters from extinction and backscatter lidar data by inversion with regularization: theory. Appl. Opt. 38, 2346–2357.

Müller, D., Wandinger, U., Ansmann, A., 1999b. Microphysical particle parameters from extinction and backscatter lidar data by inversion with regularization: simulation. Appl. Opt. 38, 2358–2368.

Müller, D., Franke, K., Wagner, F., Althausen, D., Ansmann, A., Heintzenberg, J., 2001a. Vertical profiling of optical and physical particle properties over the tropical Indian Ocean with six-wavelength lidar. 1. Seasonal cycle. J. Geophys. Res. 106 (22), 28567–28576.

Müller, D., Franke, K., Wagner, F., Althausen, D., Ansmann, A., Heintzenberg, J., Verver, G., 2001b. Vertical profiling of optical and physical particle properties over the tropical Indian Ocean with six-wavelength lidar. 2. Case Studies 106 (22), 28577–28596.

Müller, D., Mattis, I., Wandinger, U., Ansmann, A., Althausen, D., Dubovik, O., Eckhardt, S., Stohl, A., 2003. Saharan dust over a central European EARLINET-AERONET site: combined observations with Raman lidar and Sun photometer. J. Geophys. Res. 108 (D12), 4345.

Müller, D., Mattis, I., Ansmann, A., Wehner, B., Althausen, D., Wandinger, U., 2004. Closure study on optical and microphysical properties of a mixed urban and Arctic haze air mass observed with Raman lidar and Sun photometer. J. Geophys. Res. 109, D13206.

Müller, D., Mattis, I., Wandinger, U., Ansmann, A., Althausen, D., Stohl, A., 2005. Raman lidar observations of aged Siberian and Canadian forest fire smoke in the free troposphere over Germany in 2003: microphysical particle characterization. J. Geophys. Res. 110, D17201.

Murayama, T., Müller, D., Wada, K., Shimizu, A., Sekiguchi, M., Tsukamoto, T., 2004. Characterization of Asian dust and Siberian smoke with multi-wavelength Raman lidar over Tokyo, Japan in spring 2003. Geophys. Res. Lett. 31, L23103.

Rosen, J.M., Kjome, N.T., 1997. Balloon-borne measurements of the aerosol extinction-to-backscatter ratio. J. Geophys. Res. 102 (D10), 11165–11169.

Ryu, S.Y., Kim, J.E., Zhuanshi, H., Kim, Y.J., 2004. Chemical Composition of Post-Harvest Biomass Burning Aerosols in Gwangju, Korea. J. Air Waste Manage. Assoc. 54 (9), 1124–1137.

Sakai, T., Shibata, T., Iwasaka, Y., Nagai, T., Nakazato, M., Matsumura, T., Ichiki, A., Kim, Y.S., Tamura, K., Troshkin, D., Hamdi, S., 2002. Case study of Raman lidar measurements of Asian dust events in 2000 and 2001 at Nagoya and Tsukuba, Japan. Atmos. Environ. 36, 5479–5489.

Sakai, T., Nagai, T., Nakazato, M., Mano, Y., Murayama, T., 2003. Ice clouds and Asian dust studied with lidar measurements of particle extinction-to-backscatter ratio, particle depolarization, and water-vapor mixing ratio over Tsukuba. Appl. Opt. 42 (36), 7103–7116.

Santacesaria, V., Marenco, F., Balis, D., Parayannis, A., Zerefos, C., 1998. Lidar observations of the Planetary Boundary Layer above the city of Thessaloniki, Greece. Il Nuovo Gimento 21 (6), 585–595.

Sassen, K., 1974. Depolarization of laser light backscattered by artificial clouds. J. Appl. meteorol. 13 (8), 923–933.

Stull, R.B., 1988. An Introduction to Boundary Layer Meteorology. Kluwer Academic Publishers, Dordrecht.

Torres, O., Bhartia, P.K., Herman, J.R., Ahmad, Z., Gleason, J., 1998. Derivation of aerosol properties from satellite measurements of backscattered ultraviolet radiation: theoretical basis. J. Geophys. Res. 103, 17099–17110.

Veselovskii, I., Kolgotin, A., Griaznov, V., Müller, D., Wandinger, U., Whiteman, D.N., 2002. Inversion with regularization for the retrieval of tropospheric aerosol parameters from multiwavelidar sounding. Appl. Opt. 41, 3685–3699.

Wandinger, U., Ansmann, A., 2002. Experimental determination of the lidar overlap profile with Raman lidar. Appl. Opt. 41 (3), 511–514.

Wandinger, U., Müller, D., Bockmann, C., Althausen, D., Matthias, V., Bosenberg, J., Weiβ, V., Fiebig, M., Wendisch, M., Stohl, A., Ansmann, A., 2002. Optical and microphysical characterization of biomass-burning and industrial-pollution aerosols from multi-wavelength lidar and aircraft measurements. J. Geophys. Res. 107 (D21), 8125.

Whiteman, D.N., Melfi, S.H., Ferrare, R.A., 1992. Raman lidar system for the measurement of water vapor and aerosols in the Earth's atmosphere. Appl. Opt. 31 (16), 3068–3082.

Winker, D., 1999. Global observations of aerosols and clouds from combined lidar and passive instruments to improve radiation budget and climate studies. Earth Obs. 11, 22–25.